X-651-65-196

N65-29819 (ACCESSION NUMBER)
35 (PAGES)
(NASA CR OR TMX OR AD NUMBER)
(THRU)
1 (CODE)
31 (CATEGORY)
FACILITY FORM 602

NASA TM X-55266

THE NIMBUS I METEOROLOGICAL SATELLITE - GEOPHYSICAL OBSERVATIONS FROM A NEW PERSPECTIVE

BY

WILLIAM NORDBERG

GPO PRICE $ _____

CFSTI PRICE(S) $ _____

Hard copy (HC) 2.00

Microfiche (MF) .50

ff 653 July 65

MAY 1965

NASA — GODDARD SPACE FLIGHT CENTER —

GREENBELT, MARYLAND

To be presented at the COSPAR Sixth International Space Science Symposium, Buenos Aires, Argentina May 13-19, 1965

THE NIMBUS I METEOROLOGICAL SATELLITE – GEOPHYSICAL OBSERVATIONS FROM A NEW PERSPECTIVE

William Nordberg

NASA/Goddard Space Flight Center
Greenbelt, Maryland

THE NIMBUS I METEOROLOGICAL SATELLITE – GEOPHYSICAL OBSERVATIONS FROM A NEW PERSPECTIVE

by

William Nordberg

SUMMARY

29819

The Nimbus I meteorological satellite which was launched into a nearly polar, sunsynchronous orbit and was fully earth oriented carried a set of very high resolution television cameras, a directly transmitting television camera of lesser resolution and a High Resolution Infrared Radiometer. The observations of detailed cloud features during daytime, the direct transmission of such observations to local weather station via an Automatic Picture Transmission system and the measurement and pictorial presentation of earth, water and cloud temperatures from orbital altitudes at nighttime with the infrared radiometer have provided geophysical and meteorological measurements from a truly global perspective. Temperatures of ice surfaces of Antarctica and Greenland were presented in high resolution radiation pictures with accuracies of about ±2°K. Pictorial maps of cloud cover and of cloud top heights were obtained during nighttime permitting a three-dimensional analysis of the global cloud structure and inferences regarding the dynamics of weather fronts, severe storms, atmospheric circulation cells, etc. Measurements of sea surface temperatures were made in many areas of the world. Radiation patterns observed over terrain in cloudless conditions indicate the temperatures of the soil and permit inferences, in certain cases, of soil conditions such as moisture, vegetation, mineral composition, etc. The data are available for further analysis by the scientific community and a catalog of all NIMBUS observations is contained in reference (9),

CONTENTS

LIST OF ILLUSTRATIONS

THE NIMBUS I METEOROLOGICAL SATELLITE – GEOPHYSICAL OBSERVATIONS FROM A NEW PERSPECTIVE

The first photographs of the earth's surface and of large scale weather systems taken from orbital altitudes have revealed a great deal of new knowledge merely because large scale phenomena which had never been observed in their entirety were now brought within the scope of one single observation. These findings stem from a series of TIROS (Television and Infra-Red Observation Satellites) launched at the rate of about two per year since April 1960. TIROS were primarily intended to serve the operational needs of the meteorologist in the detection and tracking of storms, frontal systems and similar phenomena by means of the cloud patterns associated with these weather features. Space-borne observations of weather have also contributed to fundamental meteorological research. NIMBUS I, the first of NASA's "second generation" meteorological satellites has further advanced the potential application of such observations to meteorological research and to other fields of geophysics. The NIMBUS I system proved to be an excellent tool for remote observation of meteorological and geophysical parameters for several reasons: A sun synchronous, nearly polar orbit, a fully earth oriented, amply powered spacecraft, a set of improved and directly transmitting television cameras and a newly developed high resolution infrared radiometer (1).

THE NIMBUS I SYSTEM

NIMBUS I was launched into a nearly polar orbit on 28 August 1964 from Vandenberg Air Force Base, California. Because of a launch vehicle malfunction, an elliptic orbit (perigee 423 km and apogee 933 km) instead of the planned circular orbit at 900 km, was achieved. As planned, the orbital plane was inclined to the equator by 98.7 degrees which caused the orbit to precess around the center of the earth in synchronism with the revolution of the earth around the sun. As a consequence the relative orientation between the orbital plane and the sun remained essentially constant during the life of the spacecraft. Since at launch the orbit was chosen such that the earth-sun line lay in the orbital plane the satellite passed over most areas of the world twice every 24 hours; near local noon and near local midnight. Two stations in the United States, one in North Carolina, the other in Alaska, were used to command the spacecraft and to read out the stored telemetry and sensory data. Of the 14 to 15 orbits in a 24-hour period, eleven were expected to pass within acquisition range of one of

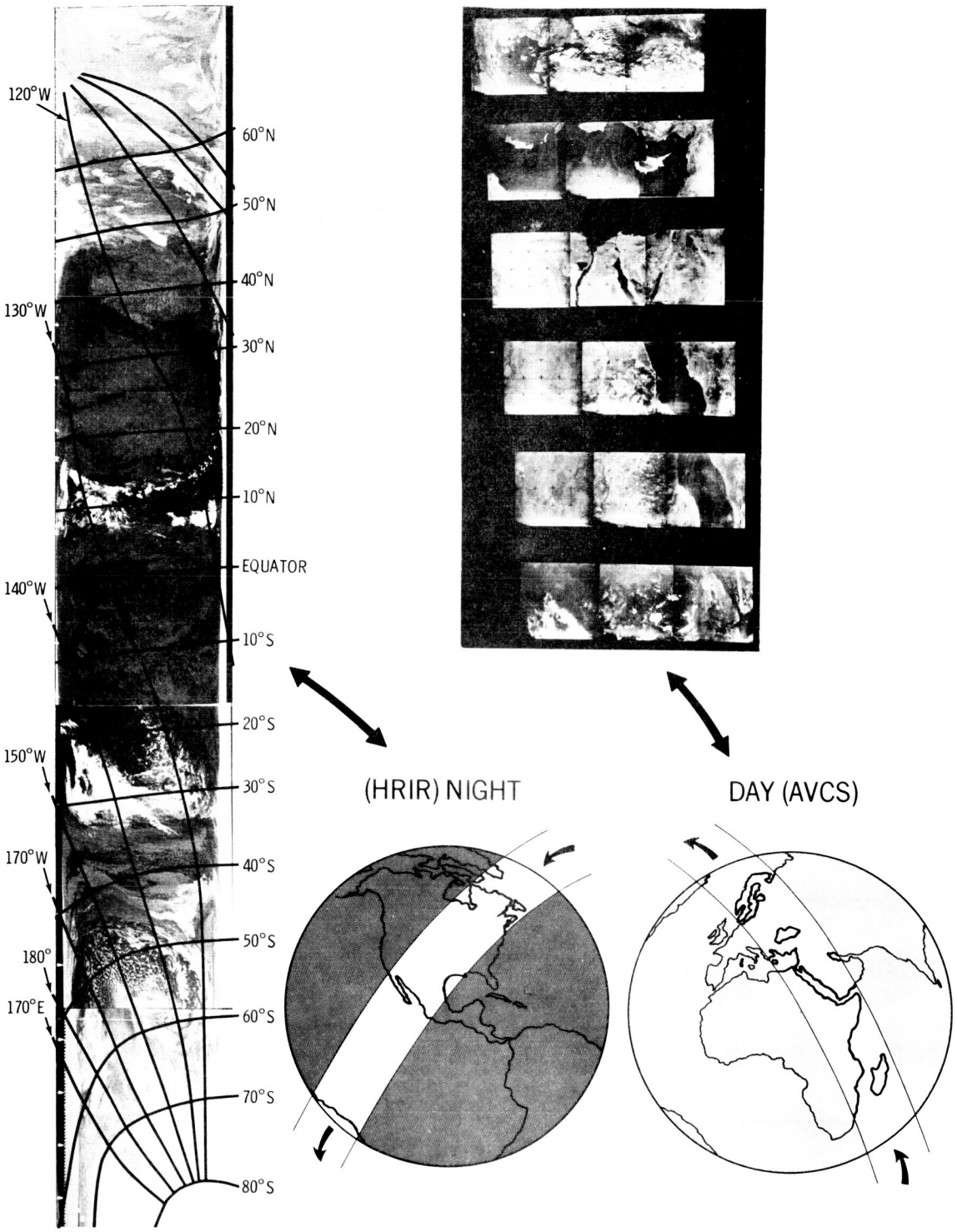

Figure 1–Extract of AVCS picture coverage during a noon time orbit of Nimbus I over the Near East on 16 September 1964 and HRIR coverage from North to South Poles across North America and the Pacific Ocean during midnight orbit, also on 16 September 1964.

the two stations. The eccentricity of the orbit, however, reduced the acquisition capability to fewer than ten orbits per day. Nevertheless, day and night photographs were obtained over 50 to 75 percent of the world on a daily basis.

The entire NIMBUS system, including a complex array of about ten spacecraft subsystems (attitude control, power supplies, telemetry, etc.) as well as data transmission and handling facilities on the ground had been designed to demonstrate the capability of delivering the complete information sensed by the spacecraft into the hands of the meteorological analyst in a format suited for immediate application. For a period of about four weeks this experiment functioned perfectly: the three-axis, active control system kept the spacecraft axis (sensor axis) oriented toward the center of the earth at all times generally within better than one degree in all three axes; the solar cell power supply continually delivered an average power of about 300 watts to the spacecraft; the spacecraft data storage and transmission system processed in excess of 50 million items of information (data words) per orbit. Pictorial presentations of the observations (Figure 1) made either during daytime with television cameras or during the night with a High Resolution Infrared Radiometer (HRIR) were generally available at the NASA NIMBUS Control Center in Greenbelt, Maryland within less than 30 minutes after the command for playback of the data was given to the spacecraft. Within these 30 minutes the information recorded in the spacecraft during any previous orbit (nominally 100 minutes of observation) were transmitted to the command station (in Alaska for example), recorded there, then transmitted further via communication circuits to Greenbelt, Maryland where appropriate geographic referencing (latitudinal and longitudinal grids) were applied automatically after which the data were transcribed onto 70 mm photographic film resulting in the strips shown in Figure 1. These strips permit a detailed analysis of weather and surface phenomena along the entire globe circling path of the satellite within less than two hours after the observations were taken. For operational meteorological applications an Automatic Picture Transmission System (APT) transmitted television observations instantly to about 50 simple and inexpensive ground stations located all over the globe. These ground stations were operated by the United States Weather Bureau, the meteorological services of the United States Armed Forces, foreign weather services and, in some cases, by educational institutions.

NIMBUS SENSORS

In the past, television cameras had proved to be the most effective instruments for observations of meteorological features from satellites. NIMBUS I carried two types of cameras: A set of three very high resolution cameras each with a field of view of about 35° and one camera with lesser resolution but

equipped with a photosensitive surface which retained a latent image sufficiently long so that images could be transmitted directly via the APT system without intermediate storage on magnetic tape. The resolution obtained with this camera permitted the recognition of cloud and terrain features of less than four kilometers in diameter. The three high resolution television cameras formed the "Advanced Vidicon Camera System" (AVCS) and yielded considerably greater detail in their pictures. Objects of linear dimensions of less than one half kilometer could be resolved. This resolution was adequate to observe practically all objects of meteorological significance. The Advanced Vidicon cameras were arranged side by side such that they covered a strip approximately 2000 km wide along the satellite track (Figure 1).

In contrast to the cameras which formed television images of reflected solar radiation the High Resolution Infrared Radiometer (HRIR) provided pictorial presentations of emitted, telluric, infrared radiation with high quantitative accuracy (2). Radiation was sensed in the narrow spectral "window" between 3.4 and 4.2 microns. A rotating mirror scanned the earth from horizon to horizon perpendicularly to the orbital path. Due to the satellite motion each successive scan line was advanced by approximately 9 km which is comparable to the linear resolution of the sensor near apogee. Because of the elliptical orbit the resolution near perigee was about 4 km. An entire nighttime half of the orbit was covered by about 2300 contiguous scans (Figure 1). The HRIR has been outstandingly successful not only in providing continuous nighttime cloud cover with a quality comparable to TIROS television pictures, but also in resolving equivalent blackbody temperatures of radiating surfaces at night within about ±1K. The HRIR was also capable of imaging cloud patterns during daylight, but the temperature resolution was lost as in that case the instrument responded primarily to reflected solar radiation which masked the telluric emission.

Mapping Blackbody Temperatures with High Resolution Radiometry

The principle of mapping cloud and terrain features by means of infrared radiation is quite simple: All objects emit electromagnetic radiation the spectral distribution and intensity of which are unique functions of the object's temperature (T) and its surface configuration. For blackbodies the intensity is a function of temperature (T_{BB}) only. This fact is expressed mathematically by Planck's law:

$$I_{BB} = \int_{\lambda_1}^{\lambda_2} (C_1/\lambda^5) \exp [1 - C_2/(\lambda T)] \, d\lambda = \int_{\lambda_1}^{\lambda_2} B(\lambda, T_{BB}) \, d\lambda \qquad (1)$$

C_1 and C_2 are constants and I_{BB} is the intensity of the radiation emitted per unit area by the blackbody surface within the wavelength interval $\lambda_2 - \lambda_1$. The NIMBUS HRIR was built to make accurate measurements of I_{BB} from which surface blackbody temperatures could be inferred. To this end λ_1 and λ_2 were selected to correspond to wavelengths of 3.4 and 4.2 microns respectively. The atmosphere is quite transparent in this spectral range. Thus, in the absence of clouds, radiation emitted by the earth's land or water surfaces reaches the satellite with only minor interference by the clear atmosphere. This interference can be corrected for according to computations made by Kunde (3). If hot (300°K) blackbody surfaces are seen through a tropical (warm and moist) atmosphere, the T_{BB} values derived from the radiation measurements must be corrected by +2 to +4 degrees K. For a dry atmosphere the correction is somewhat less and for cold surfaces (<280°K) no correction is necessary. In the presence of clouds the satellite receives radiation from the uppermost surface of the cloud. When we derive blackbody surface temperatures (T_{BB}) from the measured values of I_{BB} (equ. 1) we assume that the radiation is emitted isotropically and that the instantaneous field of view of the radiometer is filled by a surface of uniform temperature. The assumption of isotropy is not rigidly valid but must be used for lack of better knowledge of the directional variation of I_{BB}. The assumption of uniformity restricts the interpretation of the NIMBUS I surface temperature measurements to objects which are homogeneous over a distance greater than about 6 km. This is quite adequate for cloud formations associated with large scale meteorological phenomena (fronts, storms, fog layers etc.) and for many terrestrial features (deserts, ice caps, lakes etc.).

Blackbody Temperatures and Surface Temperatures

Equation 1 applies only to blackbodies. Many surfaces such as water, clouds and heavily vegetated areas are sufficiently black in this spectral region that temperatures (T_{BB}) derived from equation (1) are generally within 2°K of the actual surface temperatures (T). An error of 2°K is commensurate with the error inherent in the measurement of I_{BB}.

Some other surfaces, however, cannot be assumed as black. Laboratory measurements show that at wavelengths of about 4 microns, certain minerals and soils may absorb only a fraction (ϵ) of the radiation incident upon their surfaces. Kirchoff's law states that in this case the blackbody emission given by equation (1) must be multiplied by the same fraction ϵ to obtain the radiant emittance I_G from a non-black (grey) body:

$$I_G = \int_{\lambda_1}^{\lambda_2} \epsilon(\lambda)\, B(\lambda, T)\, d\lambda \qquad (2)$$

The fraction ϵ is the emissivity of the surface. Defining an average emissivity ($\bar{\epsilon}$) within the wavelength 3.4 to 4.2 microns we may rewrite equation (2):

$$I_G = \bar{\epsilon} \int_{\lambda_1}^{\lambda_2} B(\lambda, T)\, d\lambda = \bar{\epsilon}\, I_{BB} \tag{3}$$

Using the appropriate values for C_1 and C_2 and for λ_1 and λ_2 in Equation (1) we find that at a blackbody temperature of 290°K which is typical for the earth's surface seen by NIMBUS at low latitudes the value of I_{BB} is about 1.4×10^{-1} watts/m^2. A reduction of this value by 10 percent corresponds to a T_{BB} value of 288.2°K. This means that a surface of 290°K with an average emissivity of 0.9 emits radiation of the same intensity as a blackbody surface of about 288.2°K. Since the minimum temperature change discernible with the HRIR is about 1° to 2°K the knowledge of $\bar{\epsilon}$ in the derivation of T from I_G is important only if the emissivity is considerably smaller than 0.9.

Surface emissivities can actually be derived from HRIR daytime observations of reflected solar radiation. In this case the measured radiation intensities are not only due to surface temperatures but also due to the ability of the surfaces to reflect sunlight. The radiation intensity I_D sensed by the radiometer during daytime is the sum of the emitted grey body radiation I_G and the reflected solar radiation rI_s. The reflectivity r of practically all terrestrial surfaces is given as: $1 - \epsilon$. Thus, if we define $\bar{r}$ as the average reflectivity in the 3.4 to 4.2 micron range we may write:

$$I_D = I_G + \bar{r} I_s = \bar{\epsilon} I_{BB} + (1 - \bar{\epsilon})\, I_s \tag{4}$$

I_s is computed from the solar constant on the basis of purely geometrical considerations. A measurement of $I_D = I_s = 4.17$ watts/m^2 would result if the surface were a perfect, 100 percent effective, diffuse reflector for solar radiation at vertical incidence. For a reflectivity $\bar{r} = 0.3$, an emissivity $\bar{\epsilon} = 0.7$ and a surface temperature T = 290°K $I_{BB} = 0.11$ watts/m^2 and $\bar{r}I_s = 1.25$ watts/m^2. Hence, if the surface emissivity is smaller than 0.7, I_{BB} may be neglected and Equation (4) reduces to

$$I_D = I_s - \bar{\epsilon} I_s \tag{5}$$

If the surface temperature is less than 290°K Equation (5) is valid even for emissivities greater than 0.7. In this case the emissivity can be derived from daytime HRIR measurements without any knowledge of surface temperatures. For $\bar{\epsilon} > 0.7$

the emissivity can still be measured very accurately provided that the surface temperatures are known. For example if $\bar{\epsilon} = 0.99$ and $T = 290°K$ $I_D = 0.18$ watts/m^2; if $\bar{\epsilon} = 1.00$ (blackbody) $I_D = 0.14$ watts/m^2. The difference of 0.4 watts/m^2 is due to the term $\bar{r}I_s$ in Equation (3) and is equivalent to a blackbody temperature change of about 2°K which is just at the sensitivity threshold of the HRIR. In sunlight emissivities of 0.99 can therefore easily be discerned from blackbodies and the HRIR which was in operation during daytime for several orbits of NIMBUS I provides a very accurate method to measure large scale surface emissivities at 4 microns.

Preliminary evaluations of these daytime observations indicate that emissivities for most large scale surfaces (oceans, clouds, snow and vegetated regions) are greater than 0.9. Thus, HRIR measurements permit the worldwide mapping of actual temperatures of most surfaces during nighttime and the mapping of emissivities of non-blackbody surfaces during daytime. Global measurements of earth surface temperatures (as opposed to air temperatures measured near the ground) are of considerable value in meteorological research since these temperatures can be used as initial values in the numerical analysis and prediction of weather. At polar latitudes HRIR surface temperature maps relate to the morphology of ice formations. Such maps are both of practical application to navigation and of fundamental interest to glaciologists. Over oceans surface temperature differences may indicate the location of currents, fronts, etc. This suggests the potential use of NIMBUS HRIR observations in oceanographic research. Soil moisture content can be derived at least qualitatively from the NIMBUS HRIR observations since appreciably higher soil temperatures are measured in moist areas. Aircraft observations of emitted infrared radiation over regions of volcanic activity in Hawaii by W. A. Fisher et al. (4) have shown that underground lava beds can be detected with this technique, therefore, the NIMBUS HRIR data were also investigated for this purpose. No definite identification of any volcanic areas could be made, however, because the spatial resolution of the HRIR is apparently too coarse. Global mapping of emissivity with such coarse resolution is, nevertheless, of geological importance. Maps of emissivity obtained by the satellite establish a relationship between the small scale emission properties of various minerals and soil constituents measured on samples in the laboratory and the large scale properties of the same constituents in their natural state where they are blended with impurities, vary in grain sizes, morphology, etc. The satellite observations can be considered very useful in determining whether the distribution of mineral and similar deposits can be mapped by measurement of emitted radiation with low spectral and spatial resolution. Any findings in this area may have considerable impact on the expectations for similar measurements of lunar and planetary surfaces.

Cloud Heights

When the HRIR views a cloud covered region and a uniform cloud fills the instantaneous field of view of the radiometer, the average blackbody temperature of the cloud top surface can be derived by means of Equation (1). It is well known that in the troposphere the temperature generally decreases rapidly with altitude. It is also well known that clouds generally do not penetrate to altitudes above the troposphere where temperature increases with height. Thus, blackbody cloud top temperatures can be directly related to height (Figure 2). The deviation of cloud heights from satellite-borne radiometric measurements has been demonstrated previously with TIROS observations (5,6) but the better spatial resolution of the NIMBUS radiometer permits for the first time a detailed pictorial presentation of the vertical structure of cloud tops on a large scale. Figure 3a shows a typical example of such cloud structure over the North Pacific near midnight on 20 September 1964. In this photographic strip as in all HRIR presentations high clouds (cold temperatures) are presented as light shades of gray, while low clouds or clear areas (warm temperatures) appear dark. It is immediately apparent that the broken cloud band near the equator consists of the highest clouds in this picture, clouds in the broad band near 50°N are somewhat lower although still much higher than the large grey mass of clouds covering the North Pacific from 25 to 45°N. Only a few large, very dark regions indicating clear skies can be seen near 40°N and 140°W. The pictorial presentation of these temperature contrasts permits an instantaneous assessment of the gross features of the meteorological situation: The narrow band of very high clouds near the equator marks the Inter-Tropical-Conversion Zone, the broad band near 50°N corresponds to an intense cold front and low lying fog and stratus clouds stretching south of the front are indicated by the dark grey area. Of particular interest is the string of small, very bright (cold) spots near 137°W and 38° to 40°N. These indicate isolated, very high altitude cumulus clouds relating to thunderstorm activity. Normally, the meteorologist would never expect thunderstorm activity under the prevailing situation, especially not near midnight. However, the isolated, very high clouds definitely suggest such activity and, in this case, the validity of this interpretation was confirmed by a report from a single ship which happened to be in that area and reported towering cumuli and lightning.

A much more quantitative picture results from plotting the numerical temperatures derived by digital computers, automatically from the radiation intensities. Extracts of such automatic, numeric presentations are shown in Figure 3b. The very highest cloud in the Intertropical Convergence Zone (11.5° - 12°N and 145 - 146°W) towers to about 16 km, an altitude derived on the basis of Figure 2 from the extremely low temperature of 190°K near the center of the cloud top (Figure 3b). The fog near 40°N (Figure 3a) gives a surface temperature of 285°K

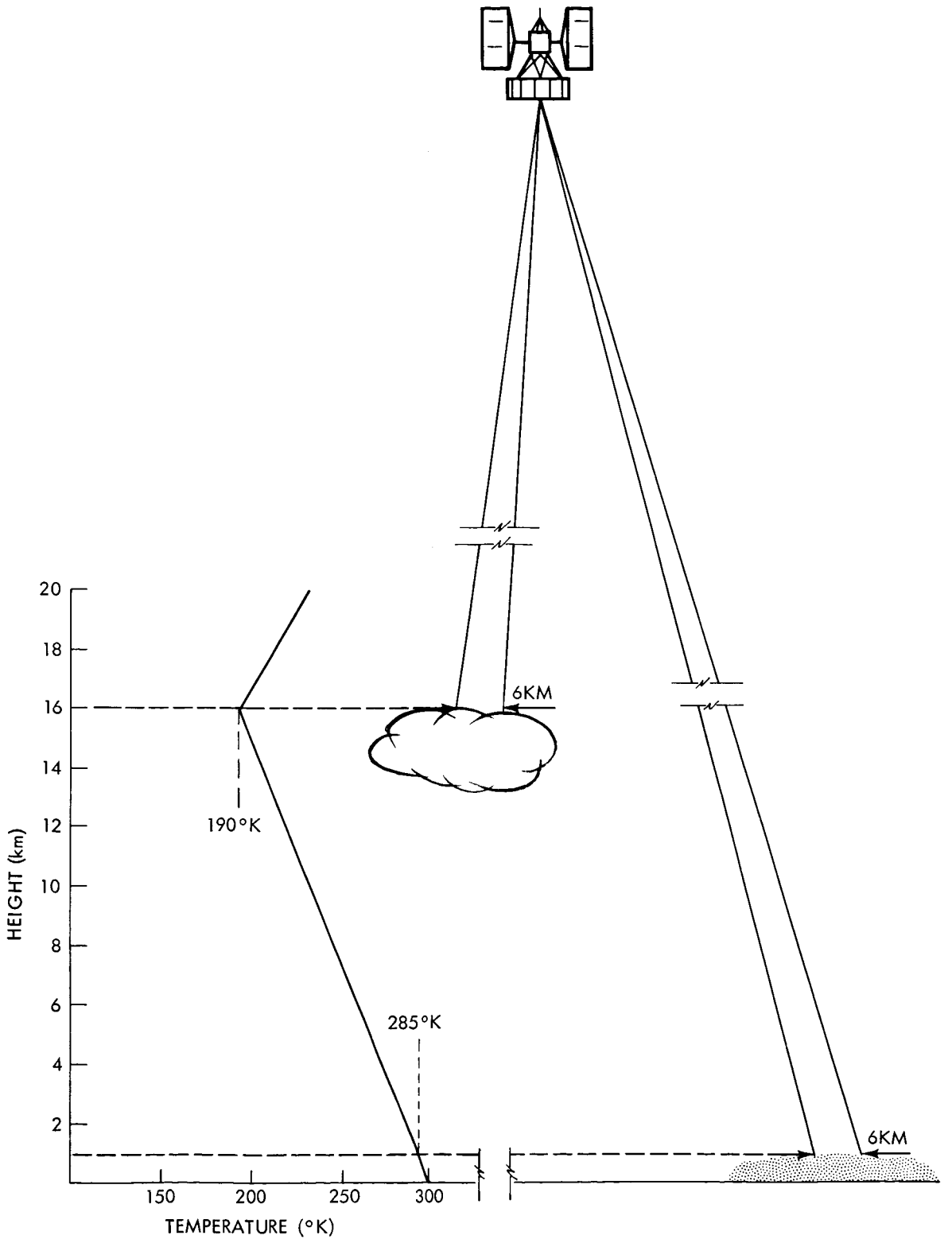

Figure 2–Typical temperature profile at tropical latitudes illustrating concept of determination of cloud top heights from satellite measurements of cloud top temperatures

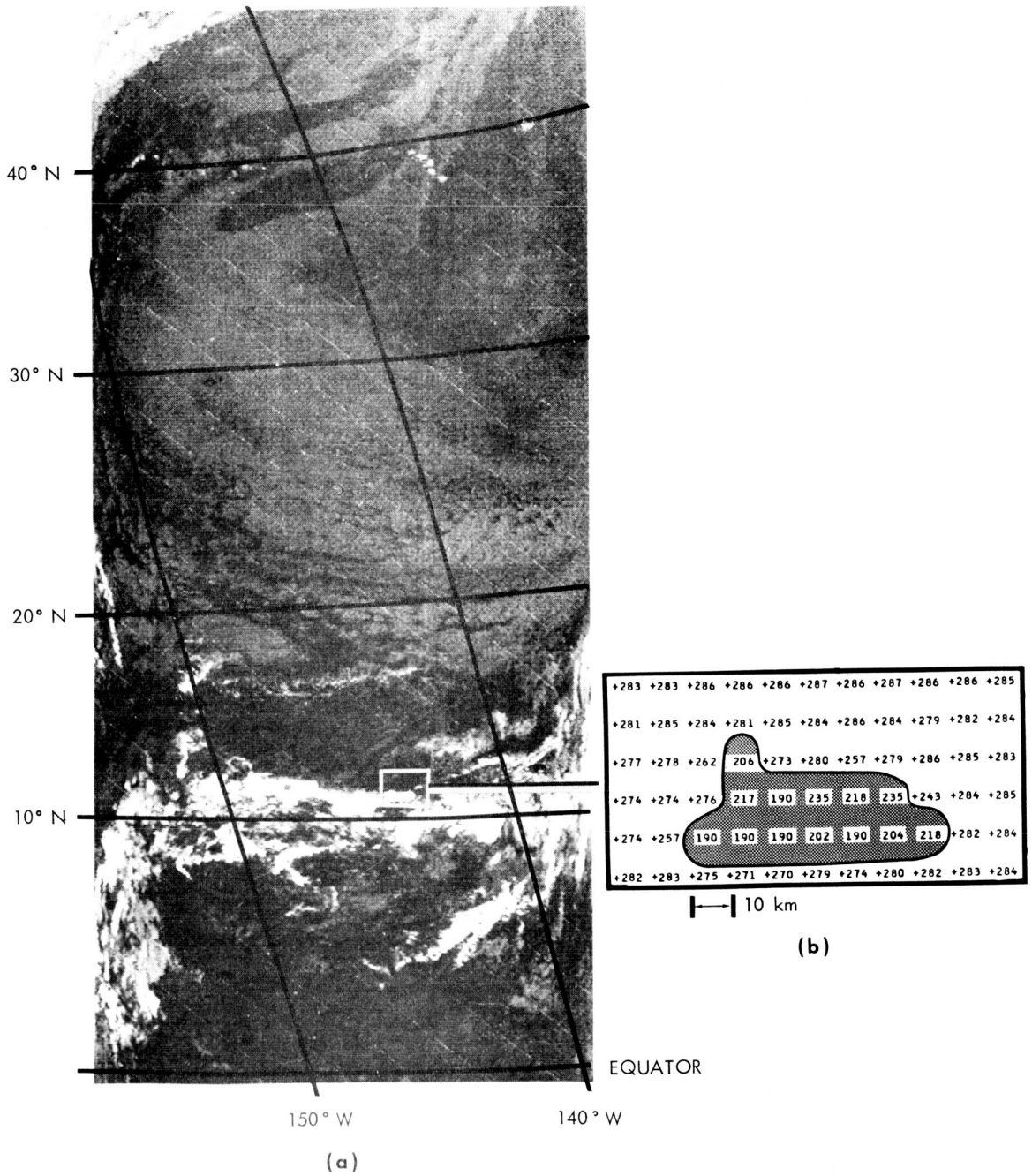

Figure 3-(a) Pictorial presentation of cloud and water temperatures over the North Pacific measured by the HRIR at midnight on 20 September 1964. (Dark shades are warm, white shades are cold). (b) Automatically produced digital map of cloud surface temperatures for a small portion of Figure 3a.

which means it reaches only to about 1 km above sea level, and the dark area in the same region corresponds to a temperature of about 293°K. The sea surface temperature measured by ships in this region were identical to that value which proves that the area was free of clouds. The accuracy of the HRIR cloud height measurements is vividly demonstrated in Figure 4a where the original analog record of one single scan across the center of Hurricane Gladys near midnight on 17 September 1964 over the Atlantic is reproduced. This scan covers a strip of 5 km width across the storm and the observed radiation intensities, expressed in degrees K, are measured along the ordinate. The blackbody temperatures were converted to height on the basis of actual temperature soundings performed by balloons in the vicinity of the storm. The corresponding heights

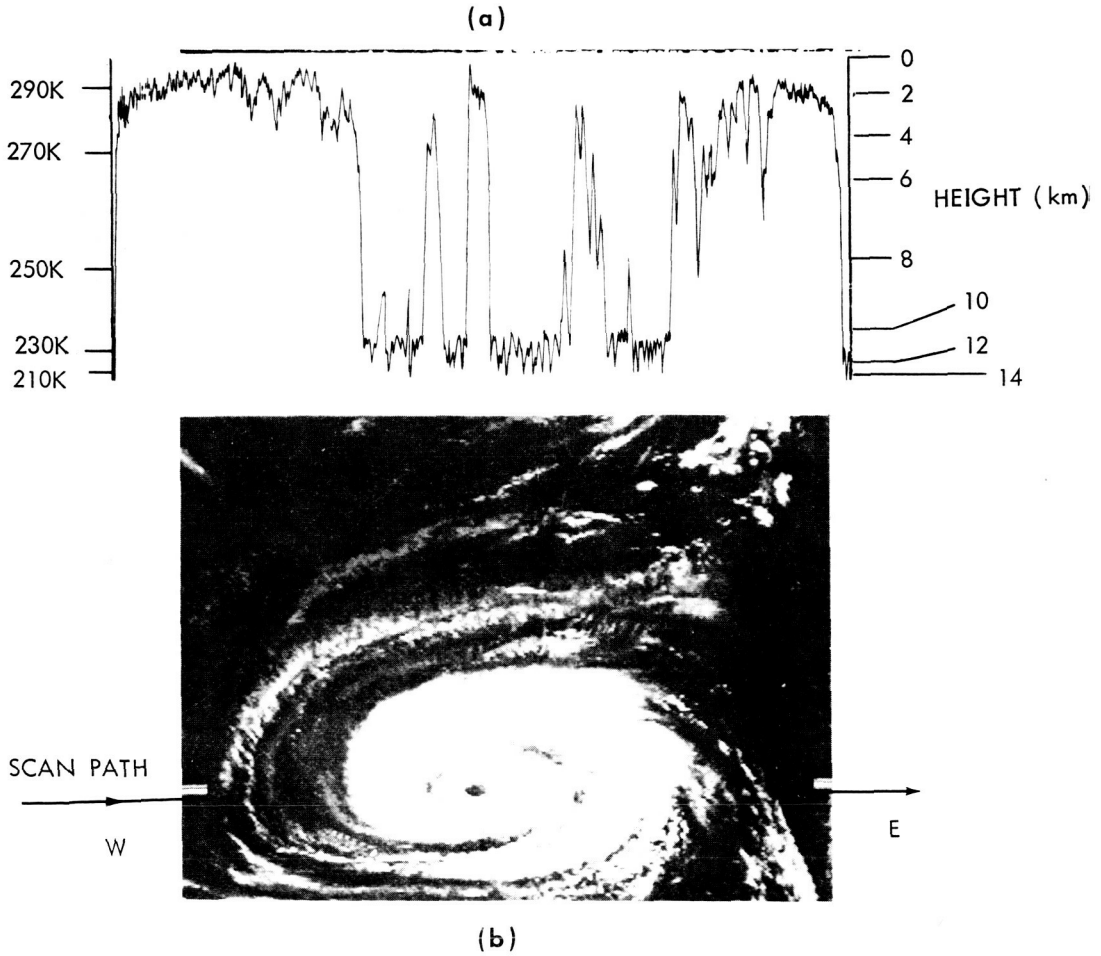

Figure 4-(a) Single HRIR scan, from horizon to horizon, across Hurricane Gladys at the location indicated in Figure 4b. (b) HRIR observation of Hurricane Gladys over the Atlantic near midnight on 17 September 1964. (Dark shades are warm, white shades are cold).

are shown along the right hand ordinate. The scan indicates temperatures near 300°K outside the storm and near 290°K in the center of the eye. The temperature of 300°K corresponds to the sea surface temperature over the clear skies outside the storm and 290°K corresponds to a height of 2 km over the eye of the Hurricane. Over the center of the spiral bands temperatures drop to 200°K corresponding to heights of 14 km. Lower clouds and partially clear skies are scanned between the spiral bands. The photographic presentation of the storm in Figure 4b is composed of a total of about 200 such scans. Detailed analysis of these highly quantitative observations of vertical cloud structure in many cases permit a much better exploration of dynamics of the atmosphere than ordinary cloud photography.

Sea Surface Temperatures

Since the blackbody assumption for water surfaces is quite valid in the 3.4 to 4.2 micron wavelength range T_{BB} values derived from the radiation intensities relate directly to water surface temperatures. In cloudless regions the HRIR, therefore, can be used to map globally the surface temperatures of various bodies of water. Figure 5 shows an HRIR picture of the southwestern United States at midnight on 30 August 1964. The darkest region in the right center corresponds to a temperature of 301°K for the water surface in the Northern Gulf of California. Applying Kunde's corrections for atmospheric absorption (3), we obtain a temperature of 303°K for the waters of the Gulf of California which is considerably warmer than the Pacific Ocean off the shore of California. There temperatures range from 293°K near the coast to about 280°K at a distance of about 200 km off shore. The low off shore temperatures indicate the presence of fog or dense haze, while the temperature of 293°K measured just west of Los Angeles is in good agreement with the temperature of 292°K measured from shipboard by the U. S. Coast Guard. Even small water features such as lakes can be clearly identified and their surface temperatures can be determined. The four black (warm) dots in the upper left corner of Figure 5 are mountain lakes in the Sierra Nevada. The southwestern most lake is Lake Tahoe, its water surface temperature was measured by the HRIR as 283°K. But, for a small body of water such as this there is a question whether the field of view of the radiometer was fully covered by the lake. The actual water temperature therefore may be several degrees higher.

The ability of the HRIR to map sea surface temperatures suggests that the course of various ocean currents such as the Gulf Stream, for example, could be detected by the satellite. Unfortunately, during the lifetime of NIMBUS I clouds obscured most areas of interest. There is, however, the possibility that certain cloud formations themselves may be related to ocean temperatures. A suggestion of this can be found in a number of cases for which Figures 6a and 6b are

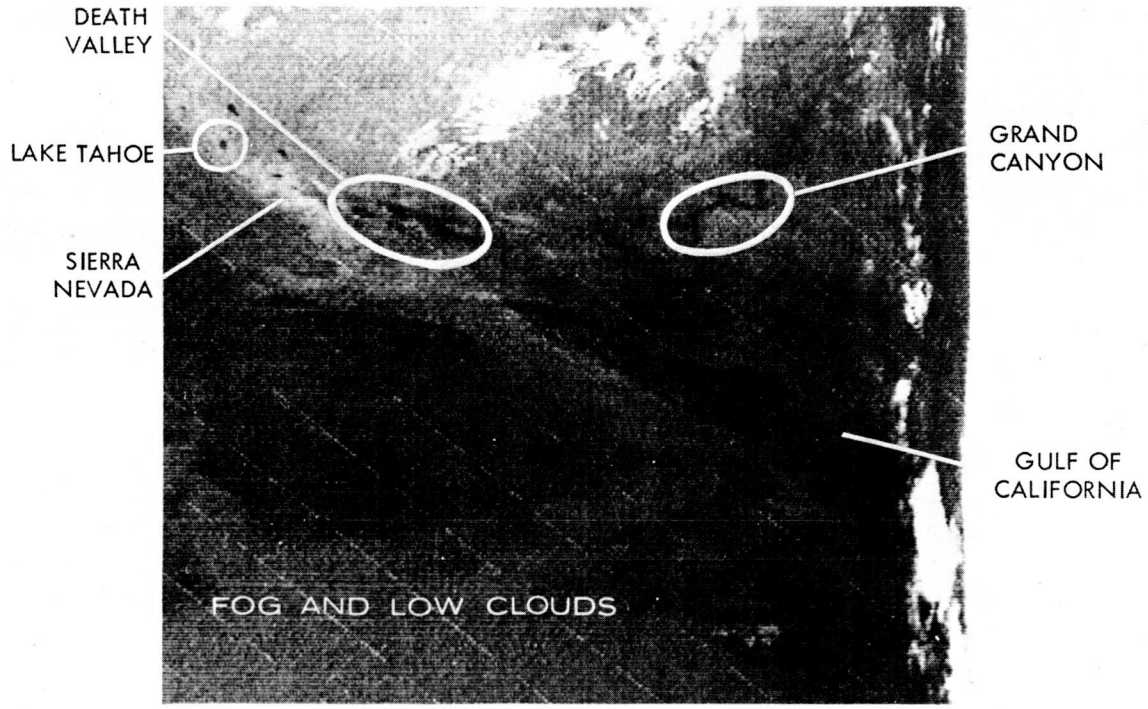

Figure 5–HRIR Ocean and terrain temperatures over the Southwestern United States near midnight on 1 September 1964. (Dark shades are warm, white shades are cold).

typical. Very low and narrow, clear streaks of open water lie between extensive low altitude stratus cloud decks over the North Pacific in Figure 6a and over the eastern Indian Ocean in Figure 6b. Here the streaks are at least 2000 km long and about 200 km wide. Although the phenomenon is apparently atmospheric it is conceivable that the cloud formations and the peculiar clearings may be influenced by ocean surface temperature differences.

Another example of satellite observed variations in sea temperatures can be found in Figure 7 where corrected sea surface temperatures, over the Mediterranean are found to range from 297°K off the coast of Africa to 290°K near Corsica. Temperatures of the Adriatic and Tyrrhenian Seas are 294°K.

Ice Formations

NIMBUS I was the first weather satellite to provide continuous observations of the polar regions. A great deal of detail in the structure of the inland ice over Antarctica, Greenland and other areas was observed with the AVCS. High resolution television observations also provided information on the morphology of

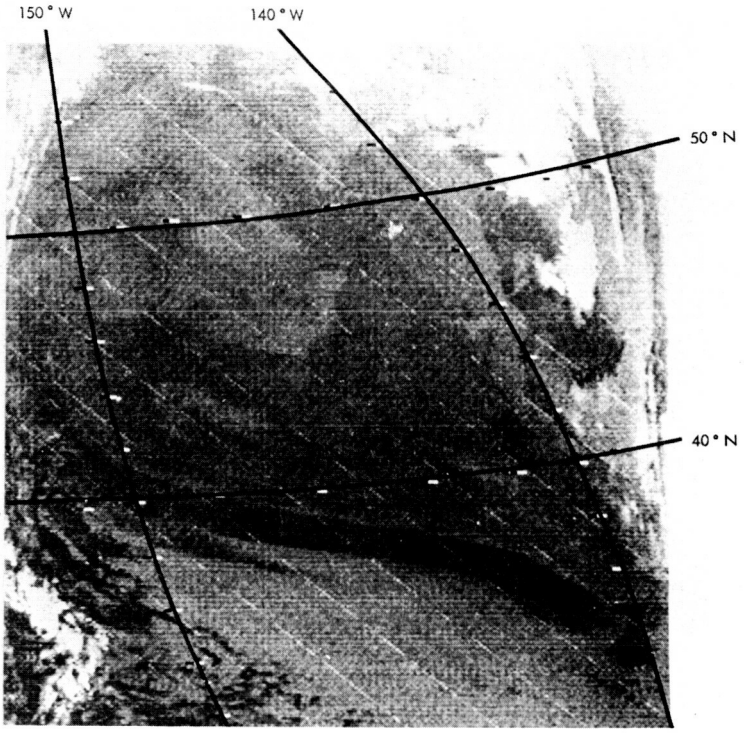

Figure 6(a)-HRIR cloud and water temperatures over the North Pacific near midnight on 30 August 1964. Clear streak of open water can be seen in the center. (Dark shades are warm, white shades are cold).

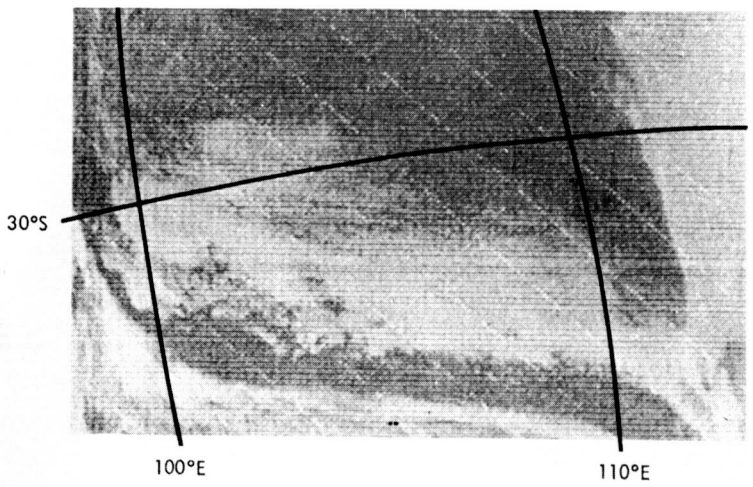

Figure 6(b)-HRIR cloud and water temperatures over the Indian Ocean near midnight on 9 September 1964. Clear streak of open water can be seen in the center. (Dark shades are warm, white shades are cold).

floating shelf ice, icebergs and similar phenomena (7). Figure 8 is a typical example of an AVCS picture showing the extent of ice cover and the structure of snow covered mountain ranges over northwestern Greenland. Details in the mountain ranges can be observed because of the pronounced shadows produced by the low elevation of the sun which generally prevails at these high latitudes.

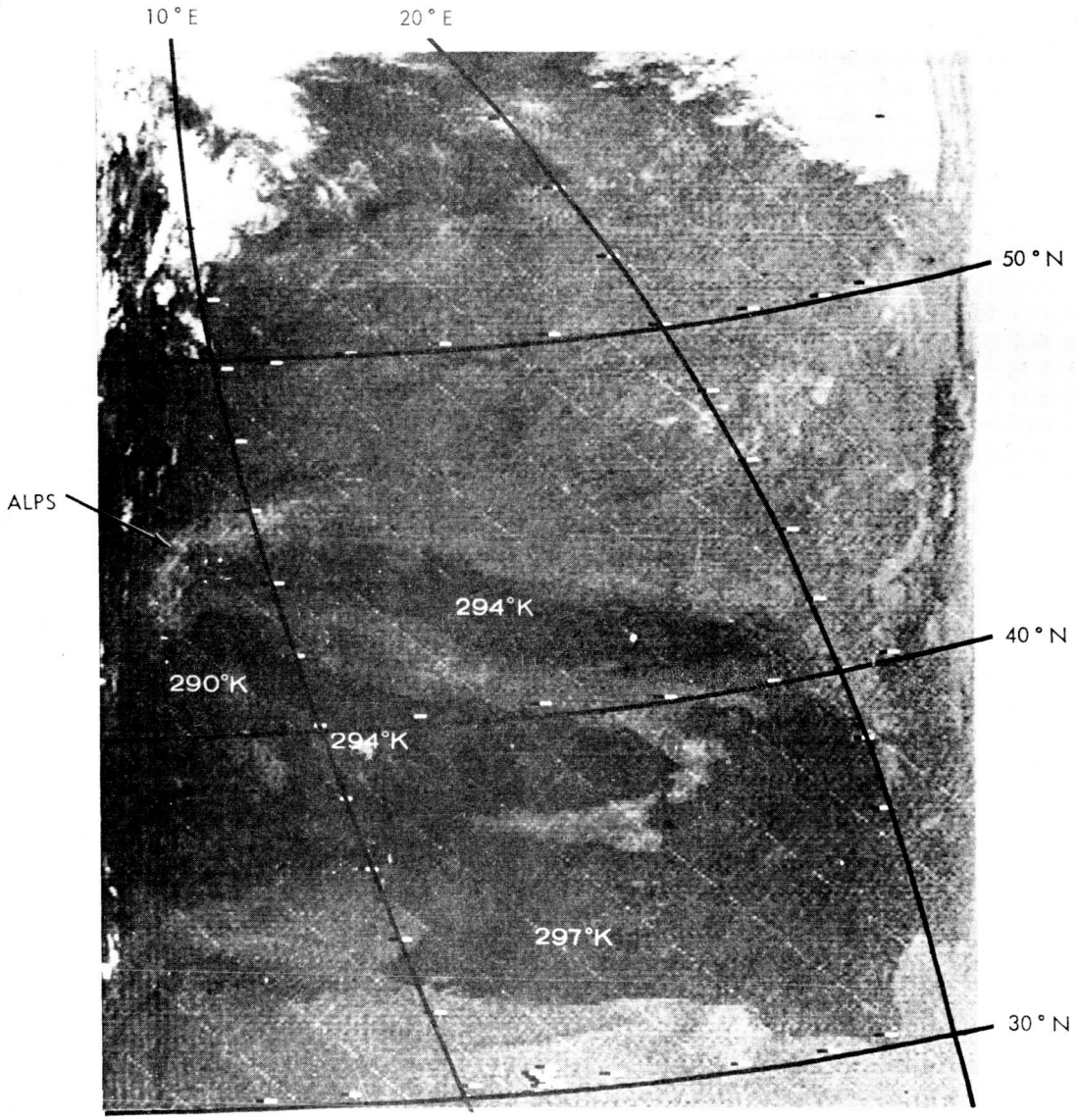

Figure 7–Temperatures over Europe observed by HRIR near midnight on 14 September 1964. (Dark shades are warm, white shades are cold).

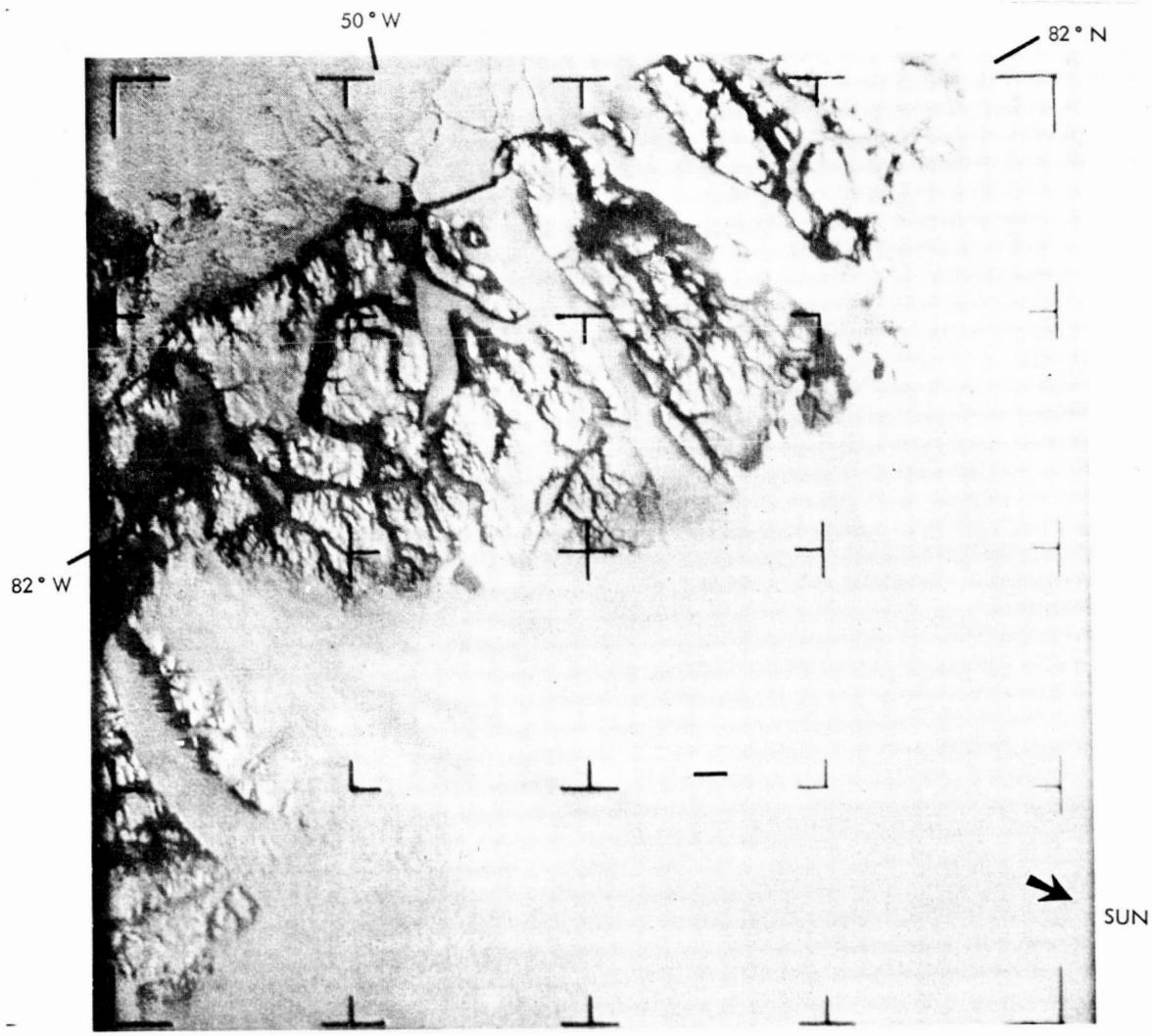

Figure 8–AVCS picture of northwestern Greenland near noon on 3 September 1964.

Figure 9 is a HRIR presentation of temperatures of Antarctic ice and water surfaces on 29 August 1964. The entire Atlantic sector of the continent is shown to be cloud free and the surface temperatures over the interior ice cap near the South Pole were determined numerically as 210-215°K. These extremely low temperatures were observed consistently during the lifetime of NIMBUS from late August to late September. Near the edge of the continent surface temperatures increase markedly to about 240°K. The edge of the continent stands out sharply in the infrared picture because a band of apparently open water about 100 km wide in spots stretches along the coast of Queen Maud Land. Maximum temperatures of these spots are about 256°K. This indicates that the full

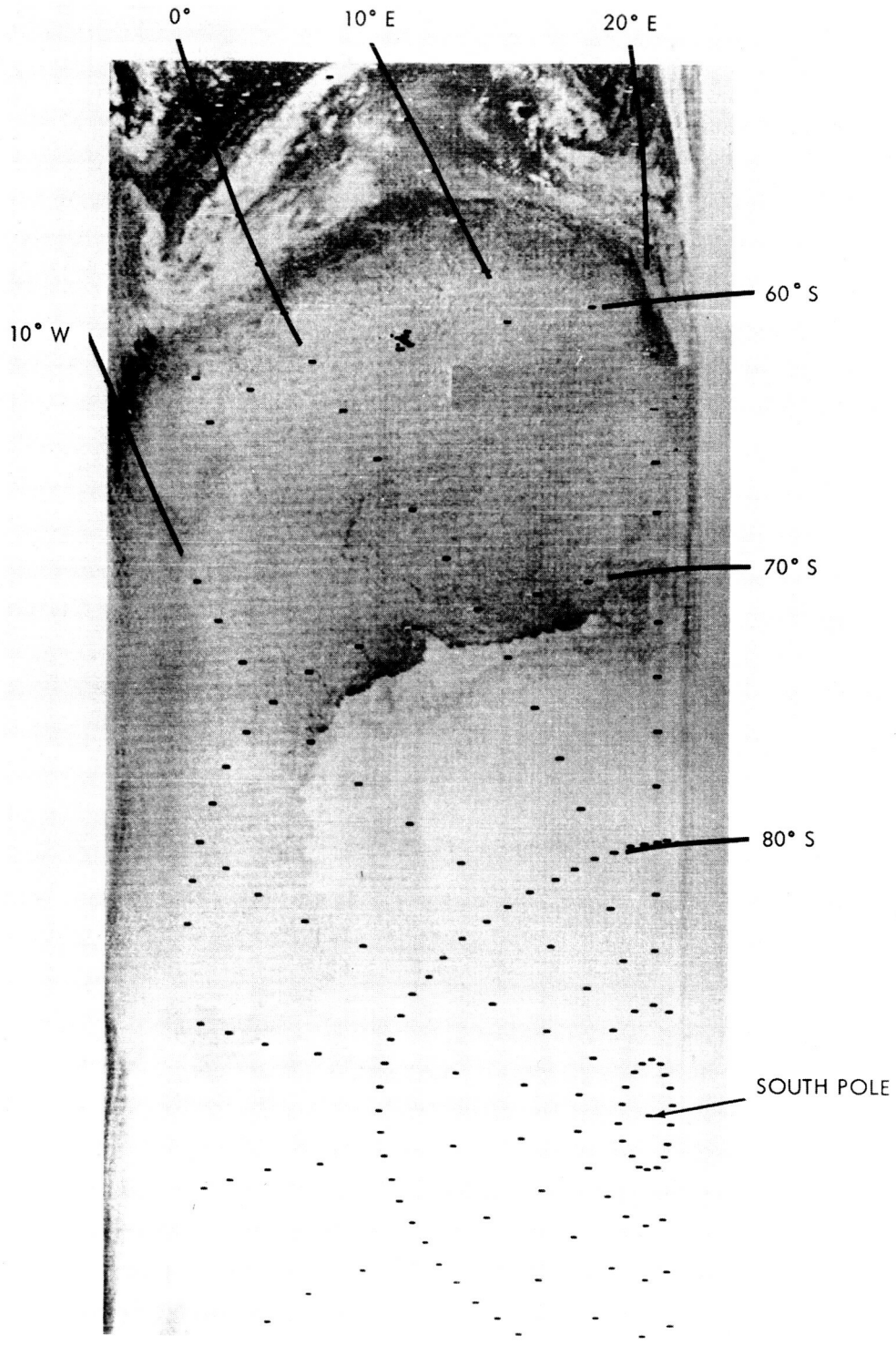

Figure 9–Temperatures over Antarctica observed by HRIR near midnight on 29 August 1964. (Dark shades are warm, white shades are cold).

instantaneous field of the radiometer was not viewing an entirely open area of water but that this band probably consists of strongly broken up ice. A wide shelf of floating ice stretches northward into the Wedell Sea and the Atlantic Ocean. The shelf ice can be easily distinguished from the inland ice because its surface temperature of 244°K is about 12°K higher. Very narrow but distinct lines of warmer temperatures are found crisscrossing the shelf. These lines obviously are due to cracks in the ice and in some cases they are over 200 km long. The ice shelf ranges up to 57°S where it is bounded by open water of temperatures of about 275°K.

Figure 10a is a HRIR picture of the Ross Ice shelf in the Pacific Sector of Antarctica. Although these observations were made four days after those shown

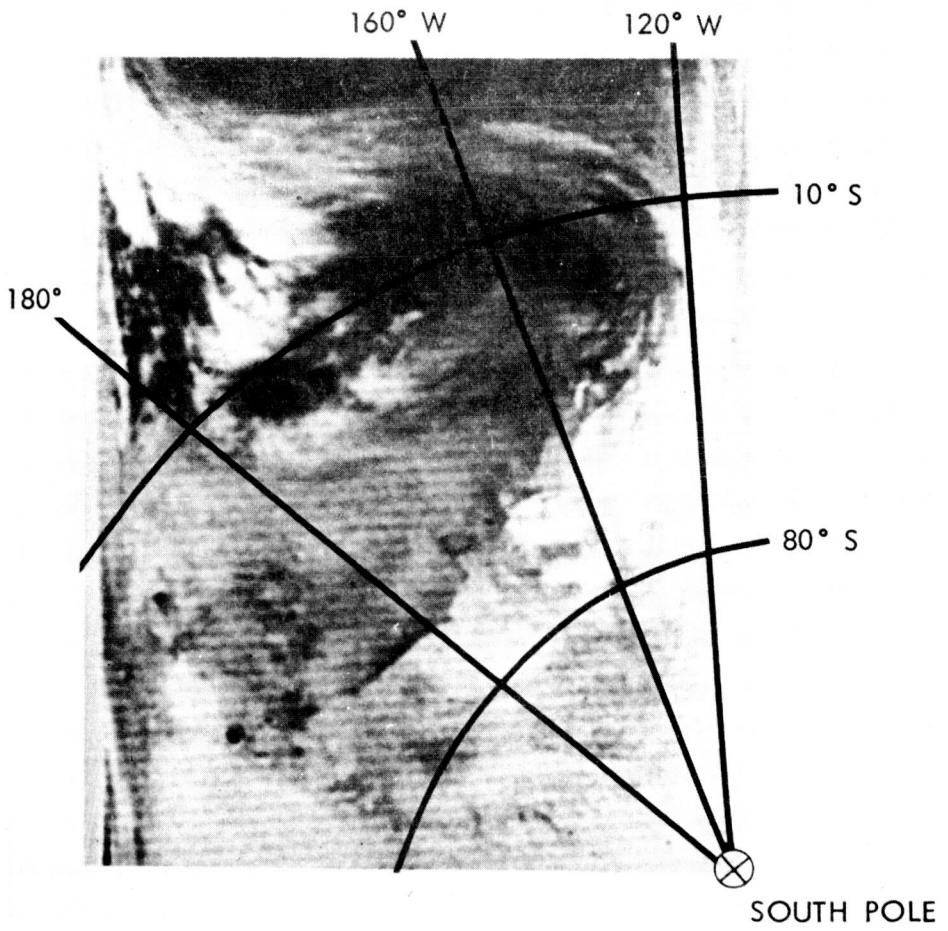

Figure 10a—Temperatures over Antarctica observed by HRIR near midnight on 1 September 1964. (Dark shades are warm, white shades are cold).

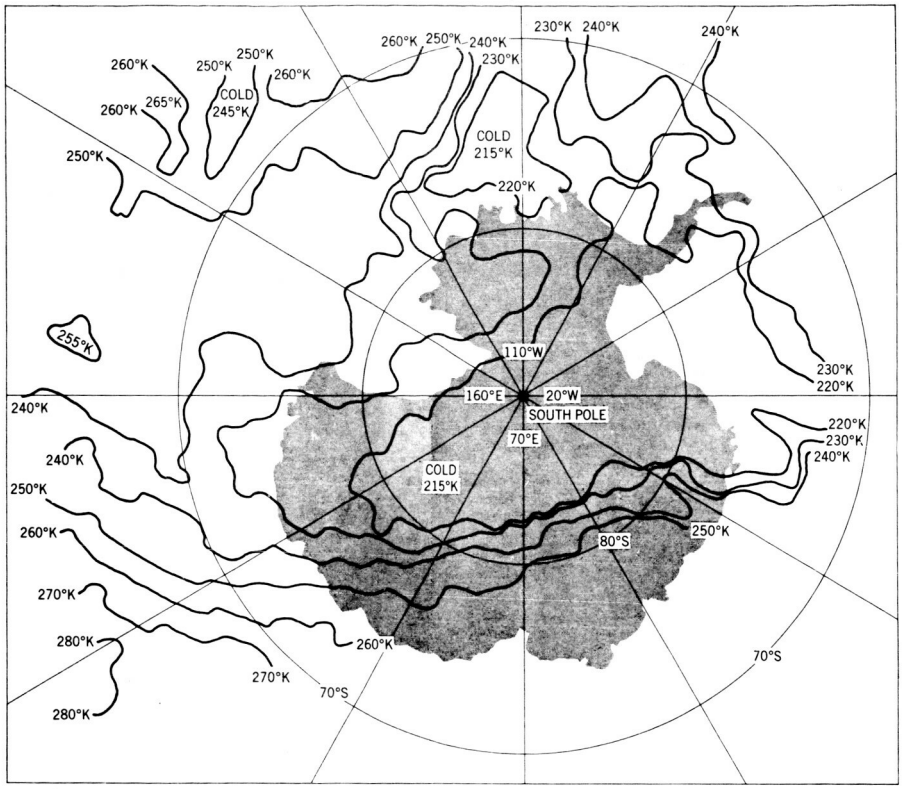

Figure 10b–Digital map of temperature contours over Antarctica for the data presented pictorially in Figure 10a.

in Figure 9, the temperatures are nearly the same over the interior ice and surface temperatures of the Ross Ice Shelf (230°K) are about 15°K lower than over the Filchner Shelf in Figure 9. Again a number of very isolated high temperature spots can be seen along the coast of Victoria Land. The most pronounced one near 76°S and 165°W has a temperature of 260°K. Since this spot is located near Mt. Erebus it was originally suspected that these isolated warm regions might be related to volcanic activity. However, as the same region was observed in subsequent HRIR pictures it became evident that some of the spots became enlarged and formed small bands along the edge of the continent. Finally on 21 September 1964 the spot near Mt. Erebus had enlarged to such an extent that it filled the entire field of view of the HRIR (Figure 11a) and the measured temperature was approximately 270°K. The fact that this is conspicuously close to the temperature of freezing water and that the same spot was photographed 12 hours later in sunlight with the AVCS (Figure 11b) leads to the definite conclusion that the spots indeed are open water. Note the identical shape of the open area in Figures 11a and 11b, despite the difference of one order of magnitude in the resolution capabilities of the AVCS and HRIR. Figure 10b is a temperature contour map of the Pacific Sector of Antarctica derived from the automatically

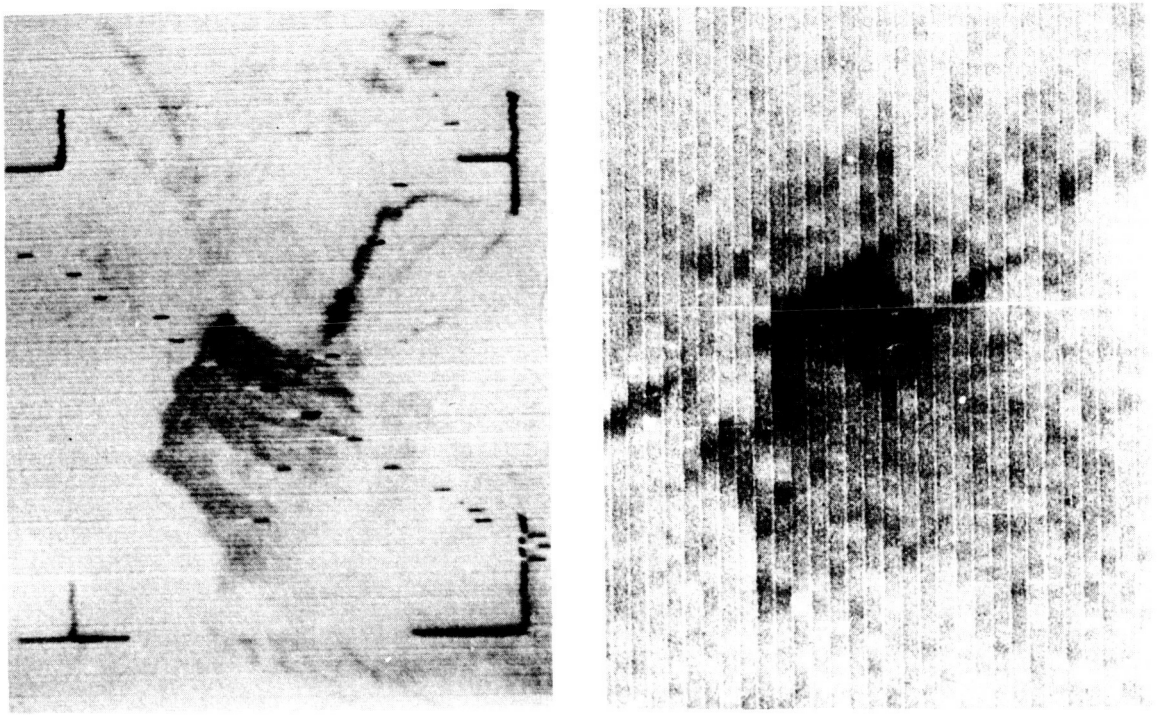

Figure 11–Comparison of warm spot observed by HRIR (a) and AVCS (b) over Antarctica on 21 September 1964.

plotted digital data for the picture shown in Figure 10a. The very low temperatures (215°K) over the high plateau surrounding the South Pole are obvious. Very tight contours toward increasing temperatures at the bottom are due to the satellite entering daylight where the HRIR detects reflected solar radiation. The high clouds seen in Figure 10a to the east of the Ross ice shelf show a temperature of about 215°K which corresponds to a cloud top altitude equal to that of the interior plateau, namely about 3000 meters. The 260°K line indicates pockets of broken ice and open water which are found in the Pacific Ocean Sector.

An HRIR picture of the Greenland ice cap is shown in Figure 12. Over clear areas the coldest region of the ice mass shows surface temperatures of about 230°K. Cloud bands can be seen extending over the southwest and eastern portion of the subcontinent. Clouds in this case appear darker (warmer) than the underlying ice. The measured cloud temperatures are about 20 degrees K warmer than the ice surface temperature. This is plausible in view of the well known "inversions" which are known to exist over the ice covered polar regions. The inversion means that over a portion of the lower atmosphere, temperatures increase rather than decrease with height thus deviating from the typical profile shown in Figure 2. The darkest portions of the region between Greenland and the large cloud mass to the south indicate clear skies over the waters of Baffin Bay and the Davis Straits. Water surface temperatures were measured near 280°K.

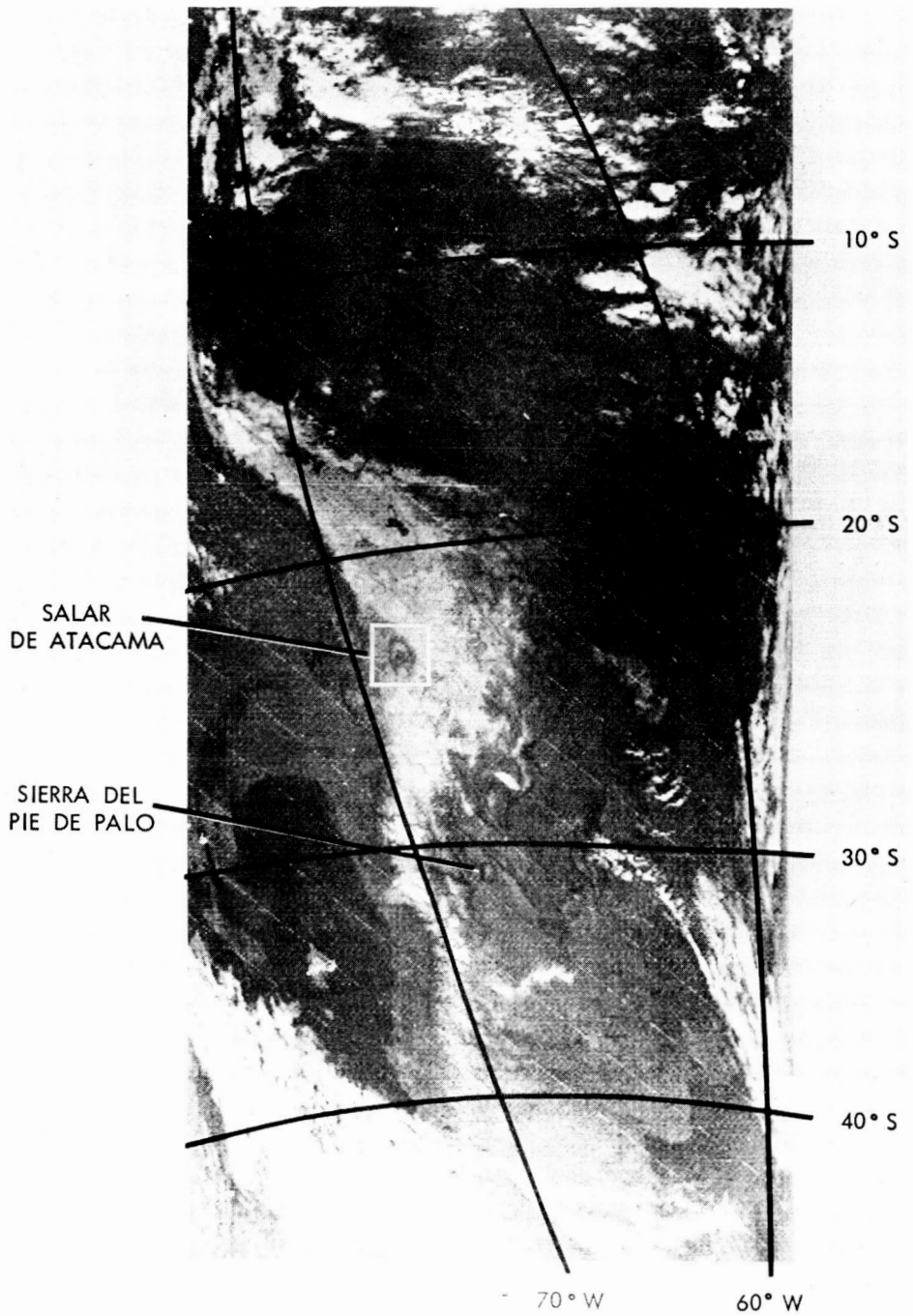

Figure 13–Temperature over South America observed by HRIR near midnight on 13 September 1964. (Dark shades are warm, white shades are cold).

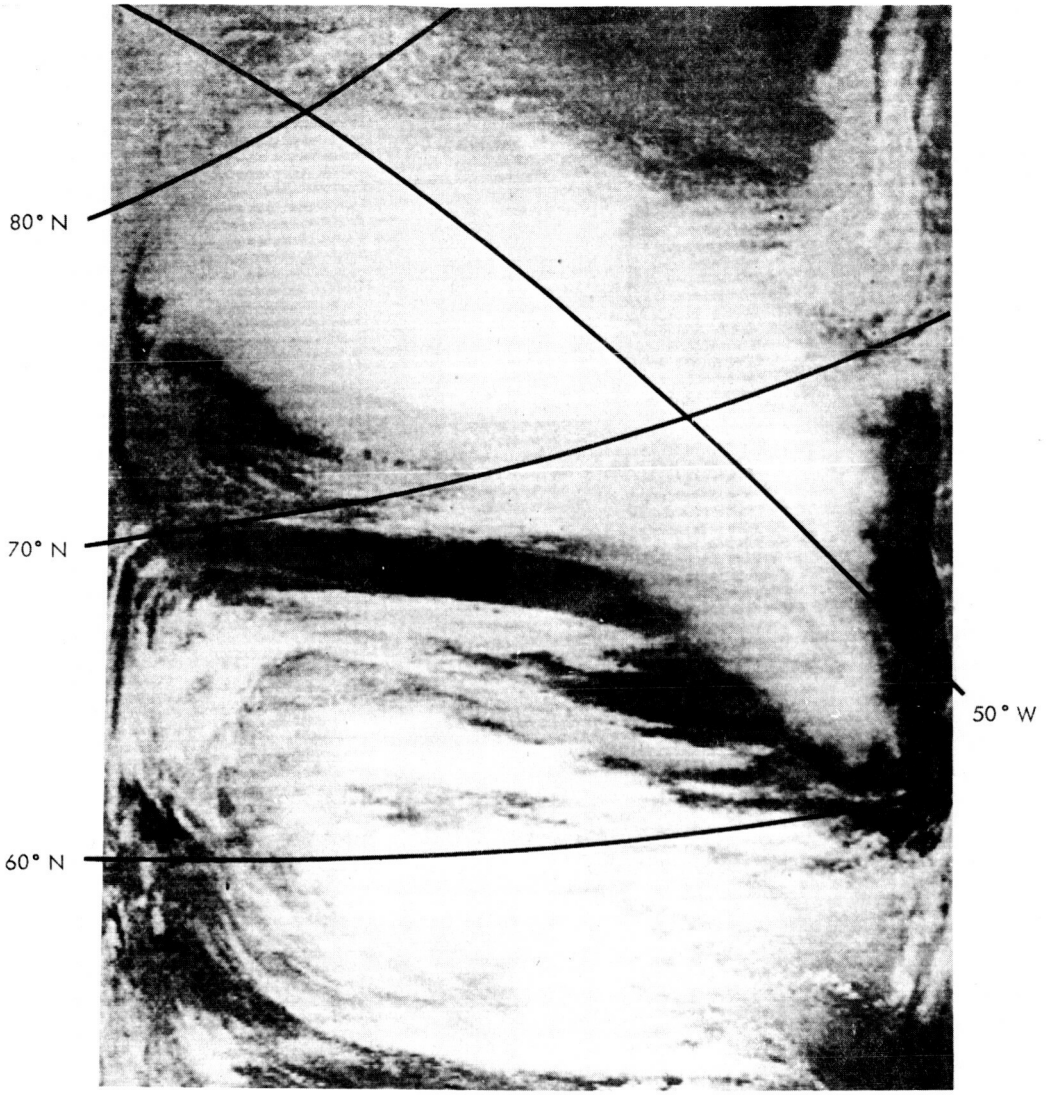

Figure 12–Temperatures over Greenland observed by HRIR near midnight on 16 September 1964. (Dark shades are warm, white shades are cold).

Terrain Features and Soil Moisture

Because solid land surfaces exist in so many varieties it is not possible to interpret the satellite measured radiation intensities as simply as in the case of water or cloud surfaces. First, a distinction must be made whether the variations in radiation intensity are due to actual ground temperature, or due to variations in emissivity. In NIMBUS I only very few examples have been found where variations in emissivities seem detectable. Figure 13 shows a very large portion

of western South America as seen by the HRIR on 14 September 1964 when much of the region was essentially free of clouds except for the Inter Tropical Convergence Zone north of 10°S, an extensive low altitude layer of stratus clouds along the entire west coast, a high altitude cloud deck off southern Chile and some smaller clouds along the eastern horizon. The broad, white (cold) band along the center of the picture corresponds to the cold, high altitude mountain ranges of the Andes. Average blackbody temperatures of 255°K are measured over the highest elevations between 28° and 32°S. To the northeast there is a remarkably rapid transition from the cold highland with average blackbody temperatures of 270°K to the very warm Amazonas Basin with blackbody temperatures of 290°K. The warm waters of Lake Poopo (19°S) and Lake Titicaca (16°S) are clearly evident in the generally cold highlands. In the plateaus to the east of the mountains (30° - 35°S) and in northern Chile (24°S) remarkable fine structure in the temperature patterns may be observed. A topographic map of the region east of Antofagasta, Chile (24°S) is shown in Figure 14. The crescent shaped figure corresponds to the Salar de Atacama, a salt flat in northern Chile. The discrete band of warm temperatures (278°K) surrounding the crescent stands out clearly in Fig. 13 while the center is quite cold (265°K). Since the entire Salar covers a region of fairly uniform altitude of about 2300 meters, there is no priori reason to assume the existence of a temperature difference between the center and the rim. Laboratory measurements by Hovis (9) show that of many common minerals tested in this spectral region pure rock salt has the lowest average emissivity. Hovis' measurements give a value of less than 0.5 for $\bar{\epsilon}$. Therefore, a blackbody temperature of less than 265°K would be measured over pure salt if the actual surface temperature were 278°K while along the periphery of the Salar rock formations at the same altitude and temperature would be detected essentially as blackbodies and produce a T_{BB} measurement which is very close to the actual temperature. The difference of over 10°K between the cold center and the warm band in Figure 13 could thus be explained. There is still a question, however, if the emissivities measured for pure salts in the laboratory are applicable to naturally impure salt deposits such as this Salar. Hovis has also measured the emissivity of natural samples of Death Valley salt deposits and obtained a value of about 0.85 for $\bar{\epsilon}$. In this case the measured blackbody temperature would be 276°K for a true surface temperature of 278°K, which is far from the difference observed over the Salar de Atacama. A question arises also because other and larger Salars in South America did not exhibit this phenomenon during this night, although the salt deposits were clearly evident in the AVCS pictures taken during daytime. HRIR observations three days earlier show the same effect much weaker over the Salar de Atacama but stronger over the Salar de Uyuni further north. Therefore, even this singular example cannot be fully explained on the basis of emissivity variations. There is still a possibility that the actual surface temperature varies in the peculiar fashion evidenced in Figure 13. Such a temperature variation could be caused by the accumulation of moisture in the ground along the

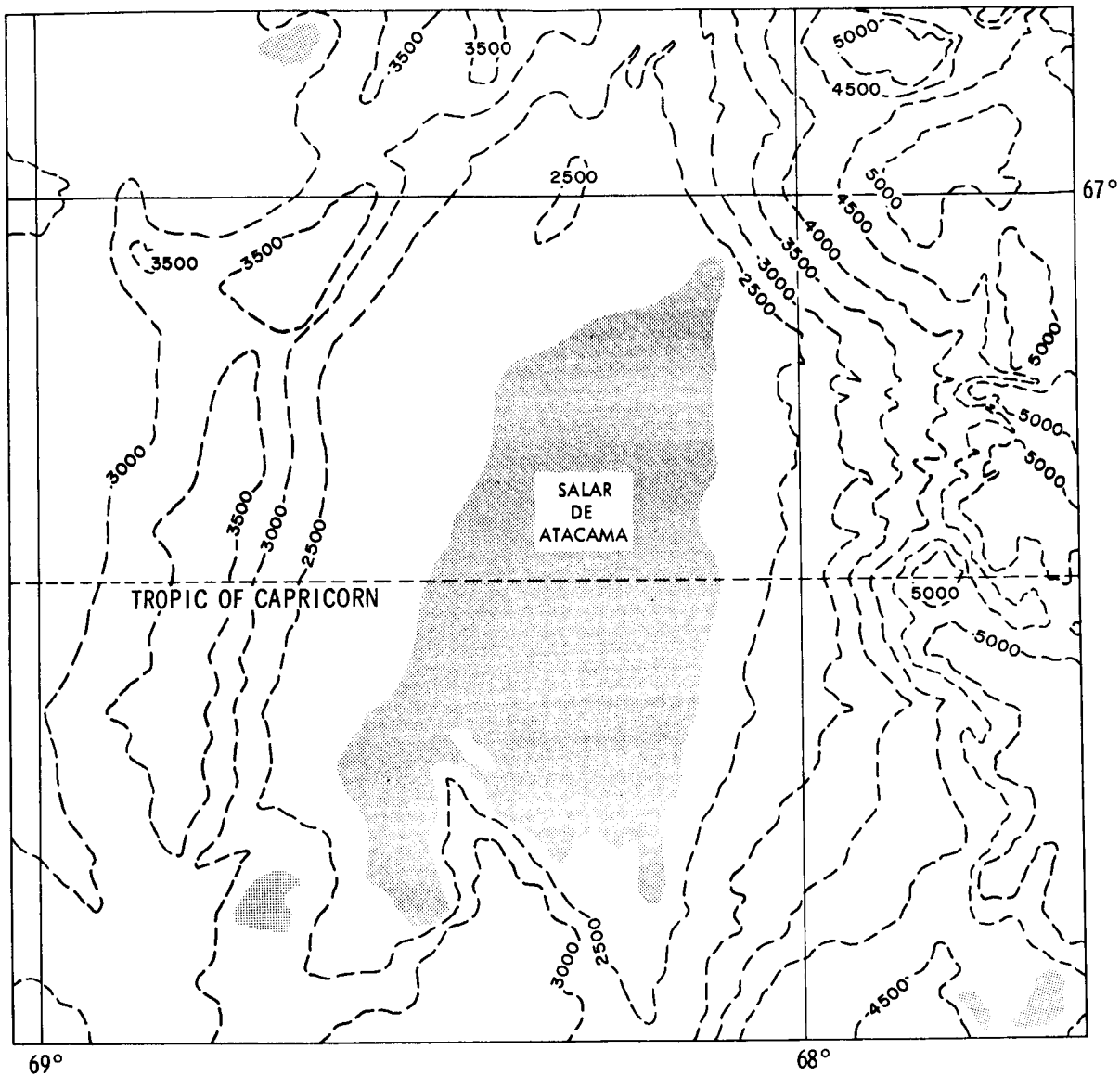

Figure 14–Topographic map of Salar de Atacama in Northern Chile.

periphery of the Salar. This accumulation may be due to drainage from the higher mountains surrounding the Salar. HRIR pictures over the deserts of North Africa and the Near East exhibit similar fine structure in the emitted radiation which demonstrates temperature variations of 10° to 15°K. Again, however, it is possible that these gradients are due to actual temperature variations rather than due to emissivity properties of the various soils. A good example can be seen over the southwestern United States in Figure 5. Here there are very dark (warmer) streaks across the Arizona and California desert regions. Midnight temperatures in these streaks range around 295°K which is about 10°K

higher than in the surrounding desert. These regions have been identified as the Grand Canyon, the Salton Sea Basin, and Death Valley. The soil in these regions remains at relatively high temperatures even at midnight contrary to the expectation that cool air from the higher surrounding desert plateaus will drain into the valleys and cool the ground. It is as yet unexplained why the very dry soil in this region does not cool more rapidly by radiation as is the case over western Argentina which will be described below.

Moisture content of the soil is also very evident in the HRIR observations. It has been very surprising that many rivers of widths of less than 1 km stand out prominently in the radiation pictures although the linear resolution of the HRIR is generally not better than 5 km. The prominence of the rivers is apparently due to the fact that the ground along these rivers is very moist and that this moisture retains solar heat absorbed during daytime much longer than drier regions. An example is shown in Figure 13. Here, the rivers in the northwest Argentinian Pampas stand out clearly as warmer (dark) bands. A conspicuously warm, almost circular band near 32°S and 69°W shows a temperature which equals that of the Rio Bermejo and Rio Zanjon further to the east. Obviously, this band cannot be a river since rivers are not known to flow in circles. Instead, we may conclude that the high temperatures in this band are due to water drainage from the Sierra del Pie de Palo, a mountain massif located in the center of the circular band. The topographic map of this area (Figure 15) indicates swamps, wells, ground water and springs around the entire mountain massif. The temperature of the dark band is about 285°K which is about equal to the free air temperature at that altitude. The lighter shades outside the band correspond to temperatures of 275°K which is about 10°K lower than the free air temperatures. This is evidence for the fact that the soil around the band has a much greater heat capacity than the soil outside the band. Low temperatures inside the band are due to the higher elevations. Moisture in the soil would retain higher temperatures during the night, thus permitting the satellite to detect the higher moisture content along the circular band and along the river beds while the dry soil loses the small amount of stored heat very rapidly by radiation during the early hours of the night. In Figure 13 for example, only vague indications can be found of the Amazonas River which is much wider than the Bermejo and Zanjon rivers that stand out so clearly. In the Amazonas Basin the entire region possesses such a large heat capacity due to its moisture and heavy vegetation that a uniform and high temperature is maintained throughout the night. Because of this fact the boundaries between water and land which include the outlines of continents cannot be distinguished in the HRIR observations in tropical regions.

An example of very close equilibrium between soil and air temperatures can be found over the Siberian Tundra as shown in Figure 16. In this figure a band of clouds, manifesting a cold front, crosses western Siberia near 60°N. Cloudless

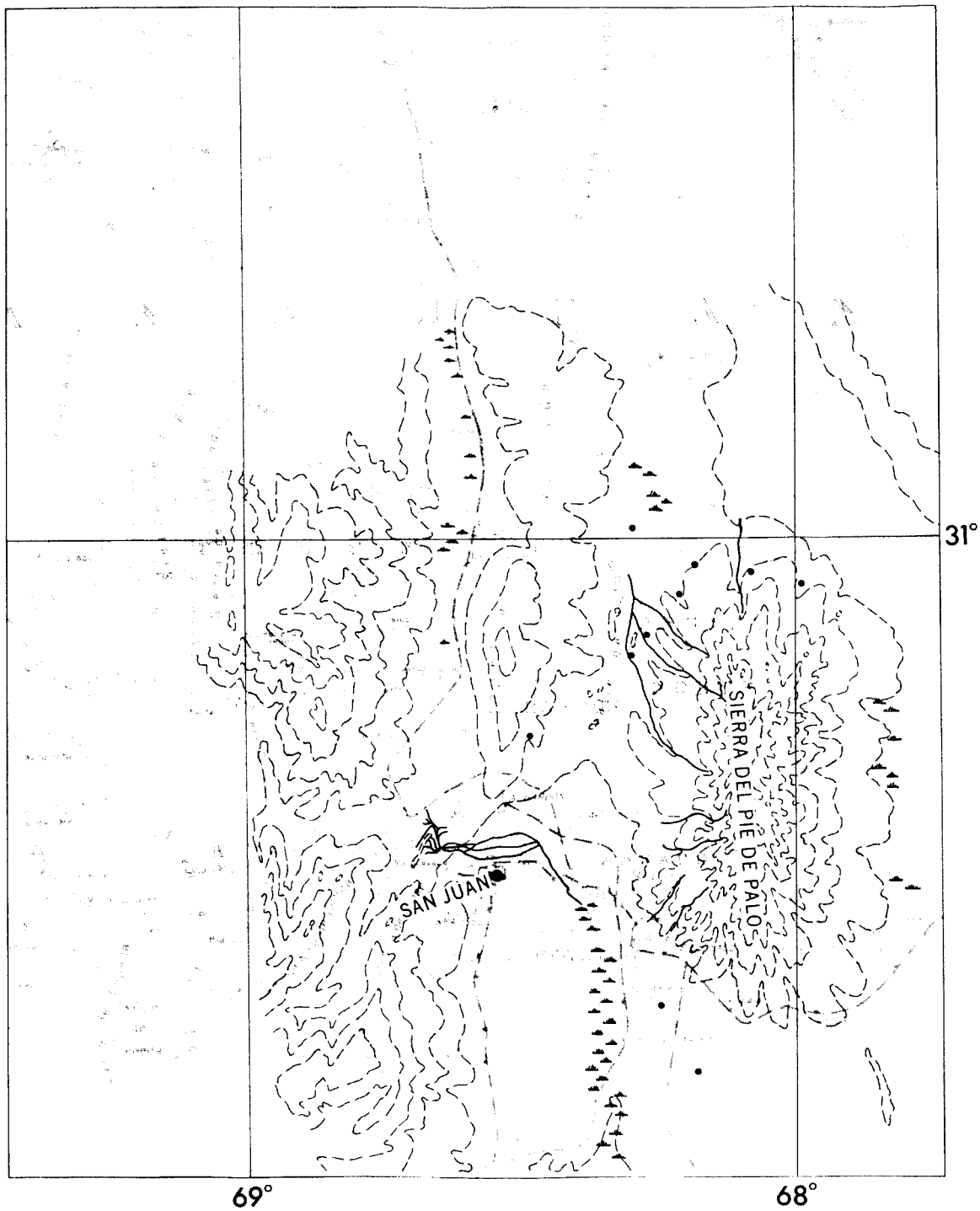

Figure 15–Topographic map of Pie de Palo mountains in western Argentina

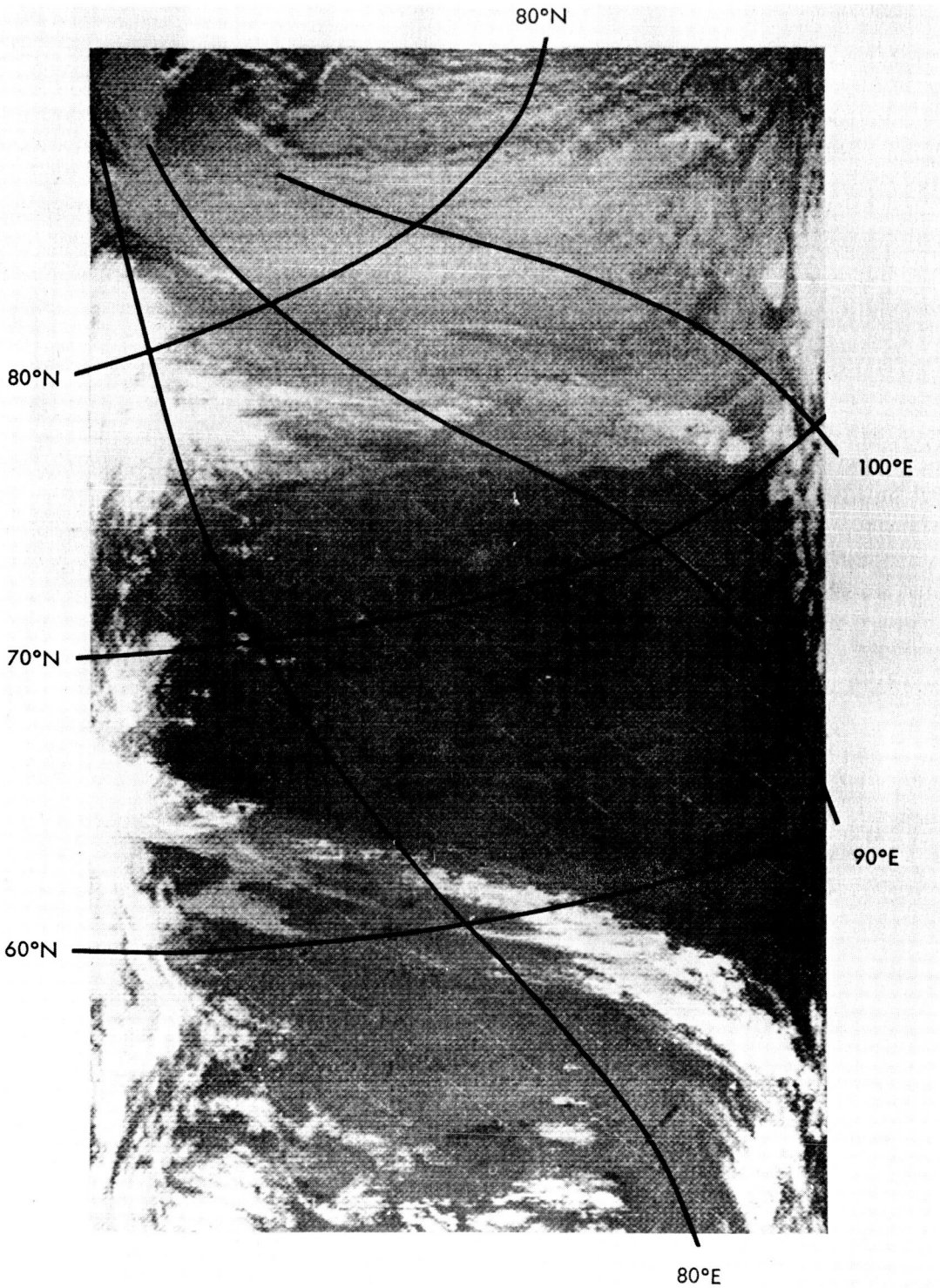

Figure 16–Temperature over Siberia observed by HRIR near midnight on 5 September 1964. (Dark shades are warm, white shades are cold).

skies prevail both to the north and south which is indicated by the clearly visible lakes and rivers on both sides of the front. Blackbody temperatures, however, are markedly different on the two sides. To the south of the front temperatures range from 277°K to about 280°K while to the northwest they are about 287°K. Analysis of surface air data provided by the Hydrometeorological Service of the U.S.S.R. show that surface air temperatures in the southern region were about 279°K while in the northwest they ranged from 283° to 288°K. This equivalence with the satellite measured soil temperatures suggests a complete equilibrium between air and soil temperatures over this region.

Thus, a variety of different geophysical and atmospheric facts can be inferred from the observation of temperature variations over the earth's terrain. Over heavily vegetated regions of the tropics the ground temperature can be measured and because of the larger heat capacity of this type of terrain its effect on air temperatures is similar as over oceans: the ground acts as a reservoir which heats or cools the air moving over it depending on its temperature. At higher latitudes, especially over dry terrain the heat capacity of the ground is so small that near midnight when solar radiation is absent, the ground temperature follows very closely the air temperature so that in most cases the satellite measured ground temperatures can be equated to the air temperatures. Singularities where this is not the case usually exhibit a very pronounced fine structure in the emission patterns. In many cases those singularities can be interpreted, qualitatively at least, as a measure of moisture content of the ground or as changes in the vegetation along the ground.

REFERENCES

(1) Nordberg and Harry Press, Bull. Am. Meteor. Soc. 45, 11, pp. 684-687 (1964)

(2) I. L. Goldberg et al., Proceedings of the Third Symposium on Remote Sensing of Environment (Univ. of Mich., Ann Arbor, Mich. (1965)), pp. 141-151

(3) V. G. Kunde, Meteorological and Geophysical Observations with the NIMBUS I Satellite (NASA, Special Publication, Wash. 25, D. C., in print)

(4) W. A. Fischer et al., Science, 146, pp. 733-742 (1964)

(5) W. R. Bandeen et al., Tellus XVI, 4, pp. 481-502 (1964)

(6) L. J. Allison et al., A Quasi Global Presentation of TIROS III Data (NASA SP-53 1964, Washington 25, D. C.)

(7) R. Popham and R. E. Samuelson, Meteorological and Geophysical Observations with the NIMBUS I Satellite (NASA Special Publication, Washington 25, D. C., in print)

(8) W. Hovis, Spectral Reflectivity of Common Minerals (to be submitted to Jour. of Appl. Optics)

(9) NIMBUS I High Resolution Radiation Data Catalog and Users Manual (Volume I), Goddard Space Flight Center, Greenbelt, Md. (1965)